A&A 582, A17 (2015)
DOI: 10.1051/0004-6361/201526644

Astronomy & Astrophysics

HD 80606: searching for the chemical signature of planet formation⋆,⋆⋆,⋆⋆⋆

C. Saffe[1,2], M. Flores[1], and A. Buccino[3,4]

[1] Instituto de Ciencias Astronómicas, de la Tierra y del Espacio (ICATE-CONICET), C.C 467, 5400 San Juan, Argentina
e-mail: csaffe,mflores@icate-conicet.gob.ar
[2] Universidad Nacional de San Juan (UNSJ), Facultad de Ciencias Exactas, Físicas y Naturales (FCEFN), San Juan, Argentina
[3] Instituto de Astronomía y Física del Espacio (IAFE-CONICET), Buenos Aires, Argentina
e-mail: abuccino@iafe.uba.ar
[4] Departamento de Física, Facultad de Ciencias Exactas y Naturales (FCEN), Universidad de Buenos Aires (UBA), Buenos Aires, Argentina

Received 1 June 2015 / Accepted 28 July 2015

ABSTRACT

Context. Binary systems with similar components are ideal laboratories that allow several physical processes to be tested, such as the possible chemical pattern imprinted by the planet formation process.
Aims. We explore the probable chemical signature of planet formation in the remarkable binary system HD 80606−HD 80607. The star HD 80606 hosts a giant planet with ∼4 $M_{\rm Jup}$ detected by both transit and radial velocity techniques, which is one of the most eccentric planets detected to date. We study condensation temperature $T_{\rm c}$ trends of volatile and refractory element abundances to determine whether there is a depletion of refractories, which could be related to the terrestrial planet formation.
Methods. We carried out a high-precision abundance determination in both components of the binary system via a line-by-line, strictly differential approach. First, we used the Sun as a reference and then we used HD 80606. The stellar parameters $T_{\rm eff}$, log g, [Fe/H] and $v_{\rm turb}$ were determined by imposing differential ionization and excitation equilibrium of Fe I and Fe II lines, with an updated version of the program FUNDPAR, together with plane-parallel local thermodynamic equilibrium (LTE) ATLAS9 model atmospheres and the MOOG code. Then, we derived detailed abundances of 24 different species with equivalent widths and spectral synthesis with the program MOOG. The chemical patterns were compared with the solar-twins $T_{\rm c}$ trends of Meléndez et al. (2009, AJ, 704, L66) and with a sample of solar-analogue stars with [Fe/H] ∼ +0.2 dex from Neves et al. (2009, A&A, 497, 563). The $T_{\rm c}$ trends were also compared mutually between both stars of the binary system.
Results. From the study of $T_{\rm c}$ trends, we concluded that the stars HD 80606 and HD 80607 do not seem to be depleted in refractory elements, which is different for the case of the Sun. Then, following the interpretation of Meléndez et al. (2009), the terrestrial planet formation would have been less efficient in the components of this binary system than in the Sun. The lack of a trend in refractory elements with $T_{\rm c}$ between both stars implies that the presence of a giant planet do not neccesarily imprint a chemical signature in their host stars, similar to the recent result of Liu et al. (2014, MNRAS, 442, L51). This is also in agreement with Meléndez et al. (2009), who suggest that the presence of close-in giant planets might prevent the formation of terrestrial planets. Finally, we speculate about a possible, ejected or non-detected, planet around the star HD 80607.

Key words. stars: abundances – planetary systems – binaries: general – stars: individual: HD 80606

1. Introduction

Main-sequence stars with giant planets are, on average, metal-rich compared to stars without planetary mass companions (e.g. Santos et al. 2004, 2005; Fischer & Valenti 2005). On the other hand, Neptune-like or super-Earth planets do not seem to be preferentially formed around metal-rich stars (e.g. Udry et al. 2006; Sousa et al. 2008). Meléndez et al. (2009, hereafter M09) have further suggested that small chemical anomalies, rather than a global excess of metallicity, are a possible signature of terrestrial planet formation. The authors showed that the Sun is deficient in refractory elements relative to volatile when compared to solar twins, suggesting that the refractory elements depleted in the solar photosphere are possibly locked up in terrestrial planets and/or in the cores of giant planets.

Most binary stars are believed to have formed from a common molecular cloud. This is supported both by observations of binaries in star-forming regions (e.g. Reipurth et al. 2007; Vogt et al. 2012; King et al. 2012) and by numerical models of binary formation (e.g. Reipurth & Mikkola 2012; Kratter 2011). These systems are ideal laboratories to look for possible chemical differences between their components, especially for physically similar stars that help to minimize the errors. For the case of main-sequence stars, Desidera et al. (2004) studied the components of 23 wide binary stars and showed that most pairs present almost identical abundances, with only four pairs showing differences between 0.02 dex and 0.07 dex. A similar conclusion was reached by Desidera et al. (2006), showing that only 6 out

⋆ The data presented herein were obtained at the W.M. Keck Observatory, which is operated as a scientific partnership among the California Institute of Technology, the University of California, and the National Aeronautics and Space Administration. The Observatory was made possible by the generous financial support of the W.M. Keck Foundation.
⋆⋆ Table 1 is available in electronic form at http://www.aanda.org
⋆⋆⋆ The reduced spectra (FITS files) are only available at the CDS via anonymous ftp to cdsarc.u-strasbg.fr (130.79.128.5) or via http://cdsarc.u-strasbg.fr/viz-bin/qcat?J/A+A/582/A17

of 33 southern binary stars with similar components present differences between 0.05 and 0.09 dex. The origin of the slight differences in these few cases is not totally clear, and a possible explanation lies the planet formation process (e.g. Gratton et al. 2001; Desidera et al. 2004, 2006).

There have been very few detailed studies of binary systems that have similar components, in which one of the stars hosts a planet. For instance, the binary system 16 Cyg is composed of a pair of stars with spectral types G1 V + G2 V, and the B component hosts a giant planet of ∼1.5 $M_{\rm Jup}$ (Cochran et al. 1997). This system has received the attention of many different works on chemical abundances in stars. Takeda (2005) and Schuler et al. (2011) suggested that both stars present the same chemical composition, while other studies found that 16 Cyg A is more metal-rich than the B component (Laws & Gonzalez 2001; Ramírez et al. 2011; Tucci Maia et al. 2014). In particular, Tucci Maia et al. (2014) also find a trend between refractories and the condensation temperature $T_{\rm c}$, which could be interpreted as a signature of the rocky accretion core of the giant planet 16 Cyg Bb. Another example is the binary system HAT-P-1, composed of an F8 V + G0 V pair, in which the cooler star hosts a ∼0.53 $M_{\rm Jup}$ transiting planet (Bakos et al. 2007). Recently, Liu et al. (2014) found almost the same chemical abundances in both stars and concluded that the presence of giant planets does not necessarily imply differences in their composition. Both members of the binary system present an identical positive correlation with $T_{\rm c}$, suggesting that the terrestrial formation process was probably less efficient in this system. Liu et al. (2014) also discuss why the chemical signature of planet formation is detected in the binary system 16 Cyg, but it is not detected in the HAT-P-1 system. The planet 16 Cyg Bb (∼1.5 $M_{\rm Jup}$) is more massive than the planet HAT-P-1 Bb (∼0.5 $M_{\rm Jup}$), which facilitates the imprint of the chemical signature in their host stars. The stellar masses in the binary system HAT-P-1 (1.16 and 1.12 $M_{\odot}$, Bakos et al. 2007) are slightly higher than in the system 16 Cyg (1.05 and 1.00 $M_{\odot}$, Ramírez et al. 2011). This implies less massive convection zones in the stars of the system HAT-P-1, i.e. more prone to imprint the chemical signature, and shorter pre-main-sequence disc lifetimes, i.e. more difficult to imprint the chemical signature. These points illustrate how complicated and challenging it could be to determine the possible effects of planet formation using stellar abundances. Then, there is a need for additional stars hosting planets in binary systems to be compared through a high-precision abundance determination.

Naef et al. (2001) first detected a giant planet around the solar-type star HD 80606 using radial-velocity measurements, which is the primary of the wide binary system HD 80606−HD 80607 (components A and B). To date, there is no planet detected around the B component. The separation between A and B stars is 21.1″ (e.g. Dommanget & Nys 2002), corresponding to ∼1000 AU at the distance of about 60 pc (Laughlin et al. 2009). This binary system is particularly notable for several reasons. Both stars present very similar fundamental parameters (their effective temperatures only differ by 67 K and their superficial gravities by 0.01 dex, as we see later). The reported spectral types are G5 V + G5 V, as described in the Hipparcos catalogue. This makes this system a new member of the selected group of binaries with very similar components. The exoplanet HD 80606 b have a period of 111.8 days and one of the most eccentric orbits to date (e = 0.927, Naef et al. 2001), probably because of the influence of the B star (Wu & Murray 2003). Besides the radial-velocity detection, Laughlin et al. (2009) reported a secondary transit for HD 80606 b using 8 μm *Spitzer* observations, while Moutou et al. (2009) detected the primary transit of the planet and measured a planet radius of 0.9 $M_{\rm Jup}$. Then, future observations of the atmosphere of this transiting planet could be compared to the natal chemical environment established by a binary star elemental abundances, as suggested by Teske et al. (2013). These significant features motivated this study, exploring the possible chemical signature of planet formation in this remarkable system.

There are some previous abundance measurements of HD 80606 in the literature. A number of elements show noticeable discrepancies in the reported values. Notably, using the same stellar parameters, the Na abundance was reported as +0.30 ± 0.05 dex and +0.53 ± 0.12 dex (Beirao et al. 2005; Mortier et al. 2013), while the Si abundance resulted in +0.40 ± 0.09 dex and +0.27 ± 0.06 dex (Mortier et al. 2013; Gilli et al. 2006). These differences also encouraged this work. We perform a high-precision abundance study analysing both members of this unique binary system with a line-by-line differential approach, aiming to detect a slight contrast between their components.

This work is organized as follows. In Sect. 2 we describe the observations and data reduction, while in Sect. 3 we present the stellar parameters and chemical abundance analysis. In Sect. 4 we show the results and discussion, and finally in Sect. 5 we highlight our main conclusions.

2. Observations and data reduction

Stellar spectra of HD 80606 and HD 80607 were obtained with the High Resolution Echelle Spectrometer (HIRES) attached on the right Nasmyth platform of the Keck 10-m telescope on Mauna Kea, Hawaii. The slit used was B2 with a width of 0.574 arcsec, which provides a measured resolution of ∼67 000 at ∼5200 Å[1]. The spectra were downloaded from the Keck Observatory Archive (KOA)[2], under the program ID A271Hr.

The observations were taken on March, 15th 2011 with HD 80607 observed immediately after HD 80606, using the same spectrograph configuration. The exposure times were 3 × 300 s for both targets. We measured a signal-to-noise ratio S/N ∼ 330 for each of the binary components. The asteroid Iris was also observed with the same spectrograph set-up achieving a similar S/N, to acquire the solar spectrum useful for reference in our (initial) differential analysis. We note however that the final differential study with the highest abundance precision is between HD 80606 and HD 80607 because of their high degree of similarity.

Our resolving power is approximately 40 percent higher than those reported in previous works (Ecuvillon et al. 2006; Gilli et al. 2006; Mortier et al. 2013). Even for a similar resolution and S/N, however, the differential line-by-line approach applied here results in a significant improvement in the derived abundances, as we show in the follwoing sections.

We reduced the HIRES spectra using the data reduction package MAKEE[3] (MAuna Kea Echelle Extraction), which performs the usual reduction process including bias subtraction, flat fielding, spectral order extractions, and wavelength calibration. The continuum normalization and other operations (Doppler

[1] http://www2.keck.hawaii.edu/inst/hires/slitres.html
[2] http://www2.keck.hawaii.edu/koa/koa.html
[3] http://www.astro.caltech.edu/~tb/makee/

correction and combining spectra) was perfomed using Image Reduction and Analysis Facility (IRAF)[4].

3. Stellar parameters and chemical abundance analysis

We started by measuring the equivalent widths (EW) of Fe I and Fe II lines in the spectra of our program stars using the IRAF task *splot*, and then continued with other chemical species. The lines list and relevant laboratory data (such as excitation potential and oscilator strengths) were taken from Liu et al. (2014), Meléndez et al. (2014), and then extended with data from Bedell et al. (2014), who carefully selected lines for a high-precision abundance determination. This data, including the measured EWs, are presented in Table 1.

The fundamental parameters ($T_{\rm eff}$, log g, [Fe/H], $v_{\rm turb}$) of HD 80606 and HD 80607 were derived by imposing excitation and ionization balance of Fe I and Fe II lines. We used an updated version of the program FUNDPAR (Saffe 2011), which uses the MOOG code (Sneden 1973) together with ATLAS9 model atmospheres (Kurucz 1993) to search for the appropriate solution. The procedure uses explicity calculated (i.e. non-interpolated) plane-parallel local thermodynamic equilibrium (LTE) Kurucz's model atmospheres with ATLAS9 and NEWODF opacities (Castelli & Kurucz 2003).

We tested the model atmospheres using the PERL[5] program *ifconv.pl*, which is available in the web[6] together with the Linux port of the Kurucz's programs. The code checks both the convergence of the stellar flux and the flux derivative in the ATLAS9 models, at different Rosseland optical depths. The convergence could be a problem in the outermost layers of models calculated with very low $T_{\rm eff}$ (~3500 K or less) and very low log g, as reported on the same page. Under these conditions, even the LTE hypothesis probably does not hold, however, the Kurucz's models used here are far from these values and have been tested using the mentioned program.

The relative spectroscopic equilibrium was achieved using differential abundances δ_i for each line i, defined as

$$\delta_i = A_i^{*} - A_i^{\rm ref}, \tag{1}$$

where A_i^{*} and $A_i^{\rm ref}$ are the abundances in the star of interest and in the reference star[7]. The same equilibrium conditions used in Saffe (2011) are written for the differential case as the following:

$$s_1 = \frac{\partial\left(\delta_i^{\rm FeI}\right)}{\partial(\chi^{\rm exc})} = 0, \tag{2}$$

$$s_2 = \frac{\partial\left(\delta_i^{\rm FeI}\right)}{\partial(EW_r)} = 0, \tag{3}$$

$$D = \left\langle\delta_i^{\rm FeI}\right\rangle - \left\langle\delta_i^{\rm FeII}\right\rangle = 0, \tag{4}$$

$$\left\langle\delta_i^{\rm FeI}\right\rangle_{\rm (INP)} - \left\langle\delta_i^{\rm FeI}\right\rangle_{\rm (OUT)} = 0, \tag{5}$$

where $\chi^{\rm exc}$ is the excitation potential and EW$_r$ is the logarithm of the reduced equivalent width. The symbol "$\langle\rangle$" denotes the abundance average of the different lines, while (INP) and (OUT) correspond to the input and output abundances in the program MOOG. The values s_1 and s_2 are the slopes in the plots of abundance vs. $\chi^{\rm exc}$ and abundance vs. EW$_r$. With this approach, Eqs. (2) and (3) show the independence of differential abundances with the excitation potential and equivalent widths (by requiring null slopes s_1 and s_2), and Eq. (4) is the differential equilibrium between Fe I and Fe II abundances. Equation (5) expresses the imposed condition to the input and output abundances in the final solution. The updated version of the program FUNDPAR searches for a solution that simultaneously verifies the conditions 2 to 5. The use of the four mentioned conditions (2 to 5) were previously tested (for the "classical" non-differential case) using 61 main-sequence stars (Saffe 2011), 223 giant stars (Jofré et al. 2015), and nine early-type stars (Saffe & Levato 2014), obtaining very similar parameters to the literature. Then, we applied these conditions for the differential line-by-line case, deriving for both stars stellar parameters in agreement with the literature and with lower errors, as we see later.

Stellar parameters of HD 80606 and HD 80607 were differentially determined using the Sun as standard in an initial approach, and then we recalculate the parameters of HD 80607 using HD 80606 as reference. First, we determined absolute abundances for the Sun using 5777 K for $T_{\rm eff}$, 4.44 dex for log g and an initial $v_{\rm turb}$ of 1.0 km s^{-1}. Then, we estimated $v_{\rm turb}$ for the Sun with the usual method of requiring zero slope in the absolute abundances of Fe I lines versus EW$_r$ and obtained a final $v_{\rm turb}$ of 0.91 km s^{-1}. We note however that the exact values are not crucial for our strictly differential study (see e.g. Bedell et al. 2014).

The next step was the determination of stellar parameters of HD 80606 and HD 80607 using the Sun as standard. For HD 80606, the resulting stellar parameters were $T_{\rm eff}$ = 5573 ± 43 K, log g = 4.32 ± 0.14 dex, [Fe/H] = 0.330 ± 0.005 dex, and $v_{\rm turb}$ = 0.89 ± 0.09 km s^{-1}. For HD 80607, we obtained $T_{\rm eff}$ = 5506 ± 21 K, log g = 4.31 ± 0.11 dex, [Fe/H] = 0.316 ± 0.006 dex, and $v_{\rm turb}$ = 0.86 ± 0.17 km s^{-1}. The metallicity of the A star is slightly higher than B by 0.014 dex. Figures 1 and 2 shows the plots of abundance vs. excitation potential and abundance vs. EW$_r$ for both stars. Filled and empty points correspond to Fe I and Fe II, while the dashed lines are linear fits to the differential abundance values.

The errors in the stellar parameters were derived as follows. We estimated the change in the "observable" quantities (i.e. the slopes s_1 and s_2 and the abundance differences shown in Eqs. (4) and (5)), corresponding to individual changes in the measured parameters $T_{\rm eff}$, log g, [Fe/H], and $v_{\rm turb}$ (50 K, 0.05 dex, 0.05 dex, 0.05 km s^{-1}). The mentioned changes in the observables are easily read in a normal execution of FUNDPAR. A similar procedure was used previously to calculate these changes (see e.g. Table 2 of Epstein et al. 2010). The differences are then used to estimate the standard deviation terms, which correspond to independent parameters in the usual error propagation. For instance, the mentioned variation of 0.05 dex in log g for HD 80606 produce a variation in D (the abundance difference between Fe I and Fe II defined in Eq. (4)) of ~0.028 dex. Then, the individual error term in log g, which only corresponds to the variation with D, is estimated in a first-order approximation as $(0.05/0.028)^2\sigma_{\rm D}^2$, where $\sigma_{\rm D}$ is the standard deviation of the D values. The D values are estimated using different Fe lines as $\sigma_{\rm D}^2 \simeq \sigma_{\rm FeI}^2 + \sigma_{\rm FeII}^2$. Then, we also take the covariance terms into account using the

[4] IRAF is distributed by the National Optical Astronomical Observatories, which is operated by the Association of Universities for Research in Astronomy, Inc. under a cooperative agreement with the National Science Foundation.

[5] PERL (Practical Extraction and Reporting Language) is a high-level interpreted programming language.

[6] http://atmos.obspm.fr/index.php/documentation/7

[7] We use the usual abundance definition $A(X) = \log(N_{\rm X}/N_{\rm H}) + 12$.

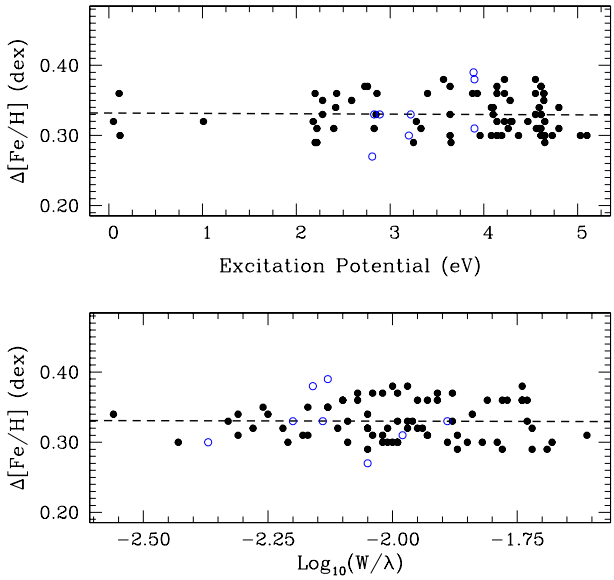

Fig. 1. Differential abundance vs. excitation potential (*upper panel*) and differential abundance vs. reduced EW (*lower panel*), for HD 80606 relative to the Sun. Filled and empty points correspond to Fe I and Fe II, respectively. The dashed line is a linear fit to the abundance values.

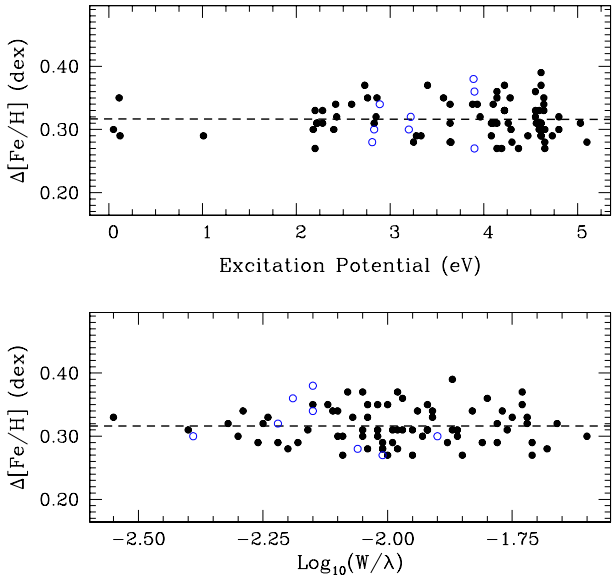

Fig. 2. Differential abundance vs. excitation potential (*upper panel*) and differential abundance vs. reduced EW (*lower panel*), for HD 80607 relative to the Sun. Filled and empty points correspond to Fe I and Fe II, respectively. The dashed line is a linear fit to the abundance values.

Cauchy-Schwarz inequality[8], which allows us to calculate the mutual covariances with the (previously calculated) individual standard deviations. With this approach, the inequality ensures that our final error adopted is not underestimated.

We repeated the process with HD 80606 as the reference star instead of the Sun, fixing the parameters of the A component to perform the differential analysis. Figure 3 shows the plots of abundance vs. excitation potential and abundance vs. EW_r, using similar symbols to those used in Figs. 1 and 2. A visual inspection of Figs. 3 and 1 shows the lower dispersion in the HD 80607 differential abundance values using HD 80606 as a reference

[8] The inequality for two variables x and y is $\sigma_{xy}^2 <= \sigma_x^2\sigma_y^2$, where σ_{xy}^2 is the mutual covariance term and σ_x, σ_y are the individual dispersions.

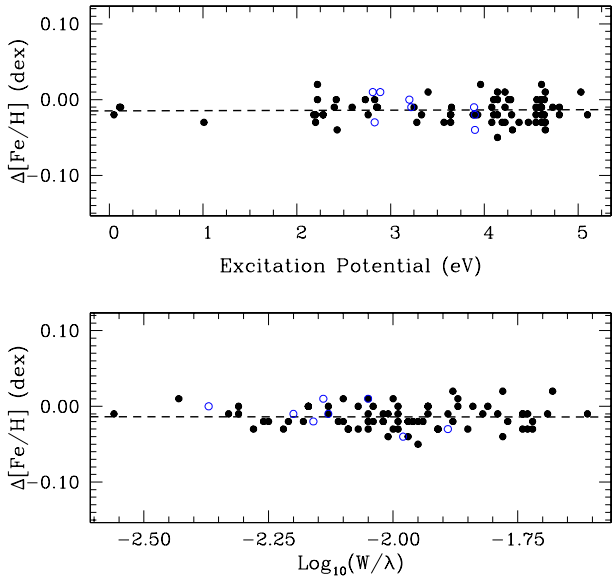

Fig. 3. Differential abundance vs. excitation potential (*upper panel*) and differential abundance vs. reduced EW (*lower panel*), for HD 80607 relative to HD 80606. Filled and empty points correspond to Fe I and Fe II, respectively. The dashed line is a linear fit to the data.

star. The resulting stellar parameters for HD 80607 yielded the same results as when we used the Sun as a reference, but with lower dispersions: $T_{\rm eff}$ = 5506 ± 14 K, log g = 4.31 ± 0.08 dex, [Fe/H] = −0.014 ± 0.003 dex and $v_{\rm turb}$ = 0.86 ± 0.07 km s^{-1}. Then, we found that the metallicity results for HD 80607 was slightly lower than the results for HD 80606 by 0.014 dex, equal to the value found using the Sun as reference.

The stellar parameters derived for the A and B stars are similar to those previously determined in the literature. Gonzalez & Laws (2007) derived [Fe/H] = 0.349 ± 0.073 dex for HD 80606, while Santos et al. (2004) derived ($T_{\rm eff}$, log g, [Fe/H], $v_{\rm turb}$) = (5574 ± 72 K, 4.46 ± 0.20 dex, 0.32 ± 0.09 dex, 1.14 ± 0.09 km s^{-1}) for HD 80606, i.e. only 1 K difference compared to our result and 0.01 dex difference in [Fe/H]. The log g and $v_{\rm turb}$ values differ by 0.14 dex and 0.25 km s^{-1}, respectively. The stellar parameters derived by Santos et al. were then adopted in other works (Ecuvillon et al. 2006; Gilli et al. 2006; Mortier et al. 2013). For HD 80607, Koleva & Vazdekis (2012) derived $T_{\rm eff}$ = 5389 ± 45 K, log g = 3.99 ± 0.18 dex, and [Fe/H] = +0.35 ± 0.06 dex, but adopting a fixed $v_{\rm turb}$ = 2.0 km s^{-1} for all the stars in their sample.

Once the stellar parameters of the binary components were determined using iron lines, we computed abundances for all remaining elements: C I, O I, Na I, Mg I, Al I, Si I, S I, Ca I, Sc I, Sc II Ti I, Ti II, V I, Cr I, Cr II, Mn I, Fe I, Fe II, Co I, Ni I, Cu I, Sr I, Y II, and Ba II. The hyperfine structure splitting (HFS) was considered for V I, Mn I, Co I, Cu I, and Ba II, using the HFS constants of Kurucz & Bell (1995) and performing spectral synthesis for these species. In Fig. 4 we show an example of the observed and synthethic spectra in the region of the line Ba II 5853.67 Å for the star HD 80606. The same spectral lines were measured in both stars. We applied non-local thermodynamic equilibrium (NLTE) corrections to the O I triplet following Ramírez et al. (2007) instead of Fabbian et al. (2009) or Takeda (2003) because those works do not include corrections for [Fe/H] > 0. The abundances for O I (NLTE) are ∼0.11 dex lower than LTE values, adopting the same correction within errors for both stars given very similar stellar parameters. We

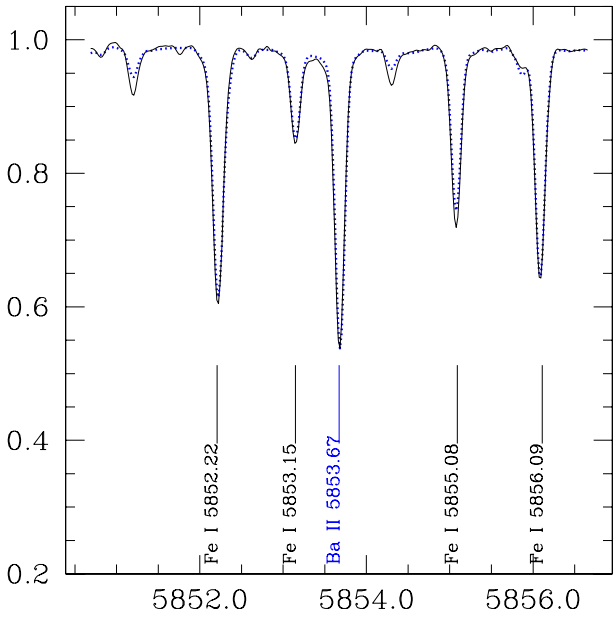

Fig. 4. Observed and synthethic spectra (continuous and dotted lines) near the line Ba II 5853.67 Å for HD 80606. Some line identifications are shown.

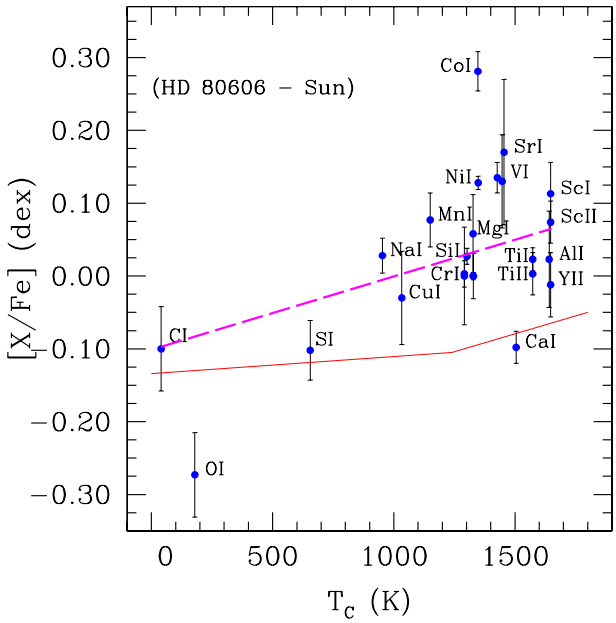

Fig. 5. Differential abundances (HD 80606 − Sun) vs. condensation temperature T_c. The dashed line is a weighted linear fit to the differential abundance values, while the continuous line shows the solar-twins trend of Meléndez et al. (2009).

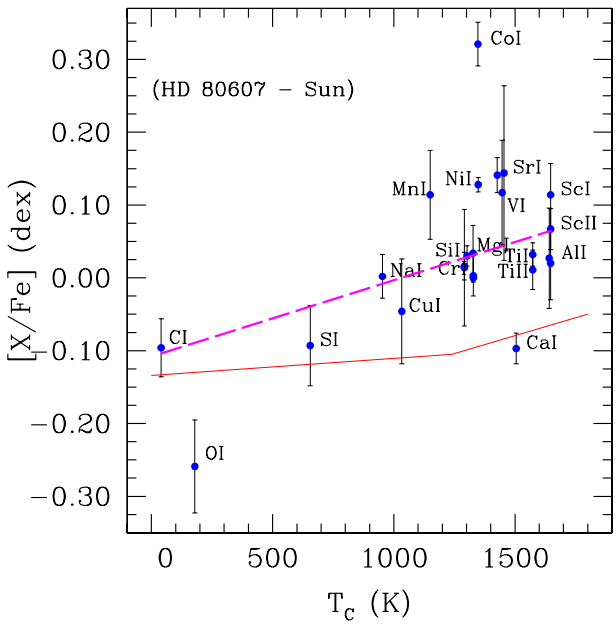

Fig. 6. Differential abundances (HD 80607 − Sun) vs. condensation temperature T_c. The dashed line is a weighted linear fit to the differential abundance values, while the continuous line shows the solar-twins trend of Meléndez et al. (2009).

also applied NLTE corrections to Ba II following Korotin et al. (2011), who clearly show that NLTE abundances are higher than LTE values for [Fe/H] > 0.

In Table 2 we present the final differential abundances [X/Fe][9] of HD 80606 and HD 80607 relative to the Sun, and the differential abundances of HD 80607 using HD 80606 as the reference star. We present both the observational errors σ_{obs} (estimated as $\sigma/\sqrt{(n-1)}$, where σ is the standard deviation of the different lines) and systematic errors due to uncertainties in the stellar parameters σ_{par} (by adding quadratically the abundance variation when modifying the stellar parameters by their uncertainties), as well as the total error σ_{TOT} obtained by quadratically adding σ_{obs}, σ_{par} and the error in [Fe/H].

4. Results and discussion

We present, in Figs. 5 and 6, the differential abundances of HD 80606 and HD 80607 relative to the Sun. We took the condensation temperatures from the 50% T_c values derived by Lodders (2003). The individual comparison between one component (e.g. HD 80606) and the Sun, is possibly affected by Galactic chemical evolution (GCE) effects because of their different chemical natal environments (see e.g. Tayouchi & Chiba 2014; Mollá et al. 2015, and references therein). On the other hand, if we assume that the stars of the binary system were born at the same place and time, we discard the GCE effects when comparing the components between them differentially; this is an important advantage of this method. Then, we corrected with GCE effects (only when comparing star-Sun) by adopting the fitting trends of González Hernández et al. (2013); see their Fig. 2, the plots of [X/Fe] vs. [Fe/H]) to derive the values of [X/Fe] at [Fe/H] ∼ 0.32 dex. A similar procedure was previously used by Liu et al. (2014) to correct the abundances in the binary system HAT-P-1 with GCE. Filled points in Figs. 5 and 6 correspond to the differential abundances for the stars HD 80606 and HD 80607, respectively. For reference, we also included in these figures the solar-twins trend of M09 using a continuous line, vertically shifted to compare the slopes. We included a weighted linear fit[10] to all abundance values, shown with dashed lines in Figs. 5 and 6. The slopes of the linear fits are similar to the trend of the solar-twins of M09 for the refractory elements.

In Figs. 5 and 6, the abundance of O I presents a low value compared to other volatile elements, while the abundances of Co I and Ca I seem to deviate from the general trend of the refractory elements (see also the next Figs. 7 and 8). For both

[9] We used the standard notation [X/Fe] = [X/H] − [Fe/H].

[10] We used as weight the inverse of the total abundance error σ_{TOT}.

Table 2. Differential abundances for the stars HD 80606 and HD 80607 relative to the Sun, and HD 80607 relative to HD 80606.

	(HD 80606 − Sun)				(HD 80607 − Sun)				(HD 80607−HD 80606)			
Element	[X/Fe]	σ_{obs}	σ_{par}	σ_{TOT}	[X/Fe]	σ_{obs}	σ_{par}	σ_{TOT}	[X/Fe]	σ_{obs}	σ_{par}	σ_{TOT}
[C I/Fe]	−0.040	0.000	0.057	0.058	−0.036	0.000	0.039	0.040	+0.004	0.000	0.028	0.028
[O I/Fe]	−0.193	0.041	0.041	0.058	−0.179	0.057	0.029	0.064	+0.014	0.031	0.020	0.037
[Na I/Fe]	−0.022	0.017	0.016	0.024	−0.048	0.028	0.011	0.030	−0.026	0.015	0.006	0.017
[Mg I/Fe]	0.078	0.050	0.019	0.054	0.054	0.033	0.017	0.038	−0.024	0.021	0.011	0.024
[Al I/Fe]	0.003	0.064	0.016	0.066	0.007	0.068	0.012	0.069	+0.004	0.007	0.009	0.012
[Si I/Fe]	0.027	0.010	0.002	0.011	0.030	0.012	0.003	0.014	+0.003	0.004	0.002	0.005
[S I/Fe]	−0.052	0.032	0.026	0.041	−0.043	0.050	0.021	0.055	+0.009	0.025	0.013	0.029
[Ca I/Fe]	−0.048	0.016	0.015	0.022	−0.047	0.016	0.013	0.021	+0.001	0.003	0.008	0.009
[Sc I/Fe]	0.073	0.035	0.023	0.043	0.074	0.041	0.013	0.043	+0.002	0.006	0.009	0.011
[Sc II/Fe]	0.034	0.014	0.025	0.029	0.027	0.017	0.021	0.028	−0.007	0.004	0.015	0.015
[Ti I/Fe]	0.033	0.012	0.009	0.016	0.042	0.011	0.009	0.016	+0.008	0.005	0.004	0.007
[Ti II/Fe]	0.013	0.022	0.019	0.029	0.021	0.020	0.017	0.027	+0.008	0.014	0.012	0.019
[V I/Fe]	0.085	0.016	0.013	0.021	0.091	0.019	0.013	0.024	+0.006	0.006	0.008	0.011
[Cr I/Fe]	0.003	0.014	0.011	0.018	0.016	0.016	0.010	0.019	+0.013	0.005	0.005	0.008
[Cr II/Fe]	0.000	0.054	0.040	0.067	0.014	0.070	0.038	0.080	+0.014	0.016	0.023	0.029
[Mn I/Fe]	−0.023	0.029	0.023	0.037	0.014	0.055	0.027	0.061	+0.037	0.012	0.014	0.019
[Co I/Fe]	0.191	0.020	0.016	0.027	0.231	0.024	0.016	0.030	+0.040	0.008	0.010	0.013
[Ni I/Fe]	0.078	0.007	0.004	0.009	0.078	0.007	0.005	0.010	−0.001	0.004	0.003	0.005
[Cu I/Fe]	−0.070	0.050	0.040	0.064	−0.086	0.060	0.040	0.072	−0.016	0.020	0.025	0.032
[Sr I/Fe]	0.120	0.050	0.086	0.100	0.094	0.060	0.106	0.120	−0.026	0.020	0.055	0.058
[Y II/Fe]	−0.002	0.028	0.034	0.044	0.030	0.027	0.042	0.050	+0.032	0.009	0.025	0.026
[Ba II/Fe]	0.190	0.050	0.040	0.064	0.177	0.060	0.040	0.072	−0.013	0.020	0.025	0.032

Notes. We also present the observational errors σ_{obs}, errors due to stellar parameters σ_{par}, as well as the total error σ_{TOT}.

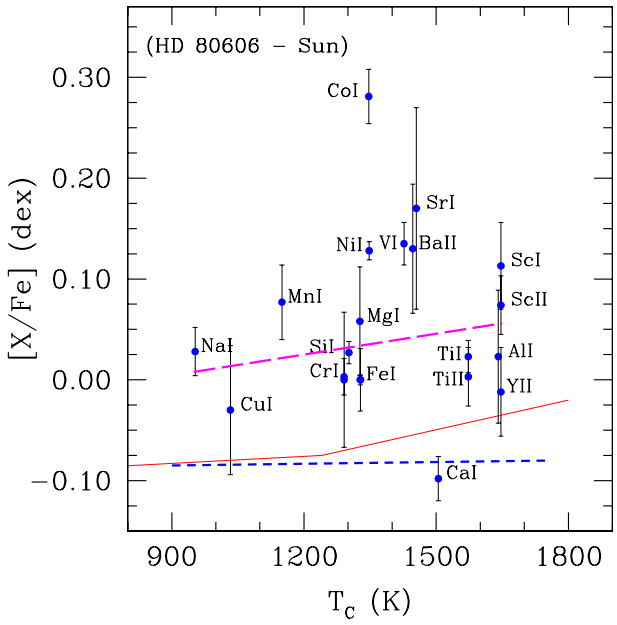

Fig. 7. Differential abundances (HD 80606 − Sun) vs. condensation temperature T_c for the refractory elements. The long-dashed line shows a weighted linear fit to the abundance values. The continuous and short-dashed lines correspond to the solar-twins trend of M09, and the solar-analogues with [Fe/H] ∼ +0.2 dex from N09.

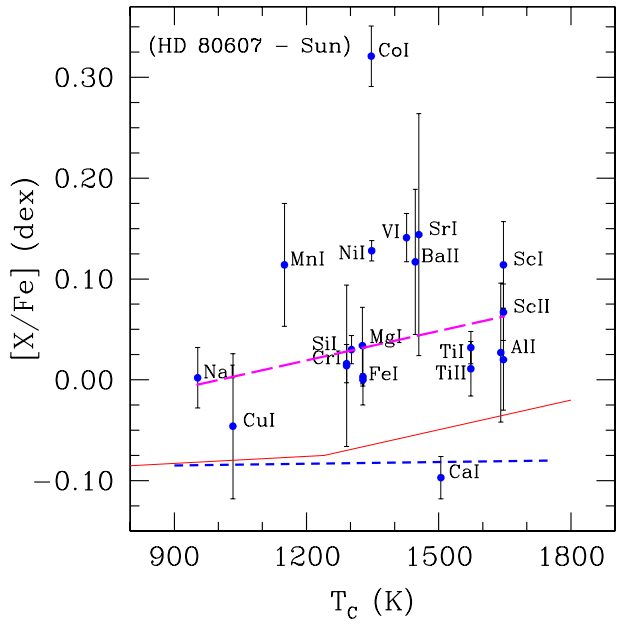

Fig. 8. Differential abundances (HD 80607 − Sun) vs. condensation temperature T_c for the refractory elements. The symbols are the same of Fig. 7.

stars, we derived the O I abundance by measuring EWs of the O I triplet at 7771 Å and applied NLTE corrections following Ramírez et al. (2007). As we noted previously, the NLTE corrections decrease the abundance in ∼0.11 dex, However, even the LTE values seem to be relatively low; we do not find a clear reason for this. The forbidden [O I] lines at 6300.31 Å and 6363.77 Å are weak and slightly asymetric in our stars. Both [O I] lines are blended in the solar spectra: with two N I lines in the red wing of [O I] 6300.31 Å and with CN near [O I] 6363.77 Å (Lambert 1978; Johansson et al. 2003; Bensby et al. 2004). Then, we prefer to avoid these weak [O I] lines in our calculation and only use the O I triplet. For the case of Co I, we take the HFS into account in the abundance calculation, however, NLTE effects could also play a role in the Co I lines of solar-type stars (see e.g. Bergemann 2008; Bergemann et al. 2010). Mashonkina et al. (2007) studied NLTE effects in the Ca I lines of late-type stars and derived higher NLTE abundances than in LTE for most Ca I lines, using a model with T_{eff} = 5500 K and

[Fe/H] = 0. For these stellar parameters, the corrections amount up to 0.08 dex with an average of ~0.05 dex, however, we caution that these studies for Co I and Ca I do not include corrections for stars with [Fe/H] > 0. Therefore, we excluded these species (O I, Co I and Ca I) from the calculation of the linear fits.

Ramírez et al. (2010, hereafter R10) studied the abundance results from six different abundance surveys and verified the findings of M09 regarding the T_c trends in the Sun and the terrestrial planet formation signature. They studied the possible dependence of the T_c trends with [Fe/H], in particular, using the sample of Neves et al. (2009, hereafter N09). The authors show that the "solar anomaly" (i.e. the T_c trend for the refractory elements in the Sun) is also observed comparing the Sun with solar-analogues at both [Fe/H] ~ −0.2 dex and [Fe/H] ~ 0.0 dex. However, for an average metallicity of [Fe/H] ~ +0.2 dex, the solar analogues from N09 shows a T_c trend for refractories similar to the Sun (see e.g. their Fig. 7). R10 interpret this result suggesting that at high-metallicity values the probability of stars with and without T_c trends should be similar, and then they find that, on average, no general trend with T_c result for the refractory elements. The authors also propose that it may be possible to distinguish metal-rich stars that show and do not show the planet formation signature from the T_c slopes of the refractory elements. Then, given that HD 80606 and HD 80607 present high-metallicity values, it also seems reasonable to compare the refractories with the solar-analogue stars with [Fe/H] ~ +0.2 dex from N09.

The differential abundances of the refractory species are shown in Figs. 7 and 8. We include in these figures the trend of the solar-analogue stars with [Fe/H] ~ +0.2 dex from N09 using a short-dashed line, which shows a near horizontal tendency. The solar-twins T_c trend of M09 is also shown with a continuous line. The tendences of N09 and M09 are vertically shifted for comparison. A weighted linear fit to the refractory species of HD 80606 and HD 80607 is presented with a long-dashed line. The refractory elements does not seem to follow a horizontal trend like the sample of N09. The general trend of refractory species for both HD 80606 and HD 80607, are more similar to the solar-twins of M09 than to the solar-analogues stars with [Fe/H] ~ +0.2 dex from N09. The Sun is depleted in refractory elements compared to the solar-twins of M09, however, the solar-analogues with [Fe/H] ~ +0.2 dex from N09 present a similar T_c trend compared to the Sun, as shown by R10. Then, following a reasoning similar to M09 and R10, the stars HD 80606 and HD 80607 do not seem to be depleted in refractory elements with respect to solar twins, which is different for the case of the Sun. In other words, the terrestrial planet formation would have been less efficient in the stars of this binary system than in the Sun.

The line-by-line differential abundances between HD 80606 and HD 80607 greatly diminishes the errors in the calculation and GCE effects in the results because they have remarkably similar stellar parameters and the same (initial) chemical composition. In Fig. 9 we show the differential abundances of HD 80607 vs. T_c but using HD 80606 as the reference star. The continuous line in this figure presents the solar-twins trend of M09 (vertically shifted), while the long-dashed line is a weighted linear fit to the refractory elements. We included an horizontal line at 0.0 dex for reference.

Most elements present slightly higher abundance values in HD 80606 compared to HD 80607, with an average difference of +0.010 ± 0.019 dex. In particular, the difference for the Fe I abundances is +0.014 ± 0.003 dex, i.e. HD 80606 is slightly more metal-rich than HD 80607. From Fig. 9, the abundances

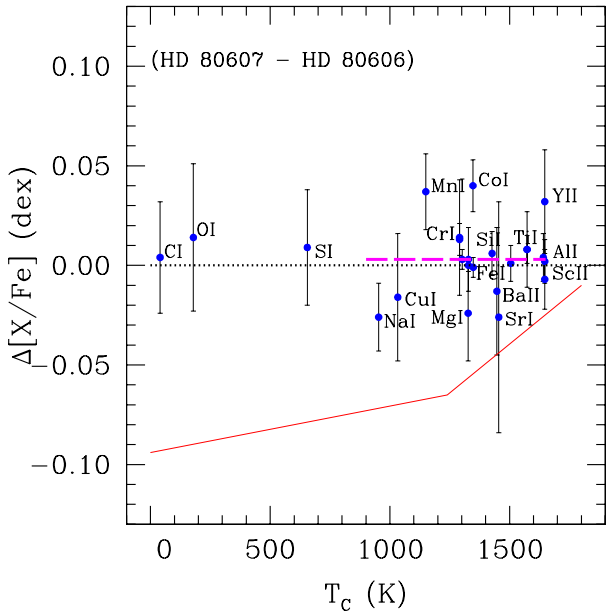

Fig. 9. Differential abundances (HD 80607−HD 80606) vs. condensation temperature T_c. The long-dashed line is a weighted linear fit to the refractory species. The solar-twins trend of Meléndez et al. (2009) is shown with a continuous line. The horizontal line at 0.0 dex is included for reference.

of the volatile does not seem to be different from the refractory elements. Their average abundances are −0.005 ± 0.005 dex and −0.011 ± 0.005 dex, i.e. almost the same within the errors. In Fig. 9, the slope of the differential abundances is −1.20 ± 16.5 × 10^{-6} dex/K for the refractory elements. For comparison, the slope of refractories between the components of the binary system 16 Cyg results in 1.88 ± 0.79 × 10^{-5} dex/K, and clearly shows a higher abundance in refractory than volatile elements (Tucci Maia et al. 2014). Then, although HD 80606 seems to present a slightly higher Fe I abundance than HD 80607, there is no clear difference between refractory and volatile elements nor is there a significative trend with T_c. This would imply that there is no clear evidence of terrestrial planet formation in this binary system. Similarly, Liu et al. (2014) did not find a trend with T_c in the binary system HAT-P-1 and concluded that the presence of a giant planet does not neccesarily introduce a chemical signature in their host stars. This is in line with some previous literature works, who propose that the presence of close-in giant planets might prevent the formation of terrestrial planets (Meléndez et al. 2009; Steffen et al. 2012). For the case of eccentric giant planets, numerical simulations also found that the early dynamical evolution of giant planets clear out most of the terrestrial planets in the inner zone (Veras & Armitage 2005, 2006; Raymond et al. 2011).

4.1. A planet around HD 80607?

Up to now, there is no planet detected around HD 80607. The photometry of HD 80607 is relatively flat, i.e. a transit-like event is not observed (Fossey et al. 2009; Pont et al. 2009). To our knowledge, this object is not included in the current radial velocity surveys.

However, given the abundance results of this study and the confirmed presence of a giant planet (with very high eccentricity) only around HD 80606, we can speculate about a possible planet formation scenario in this binary system. The occurrence of planets was fit by Fischer & Valenti (2005)

using a power law as a function of the metallicity: $P = 0.03\ (N_{Fe}/N_H)^2/(N_{Fe}/N_H)^2_\odot$. Then, the probability increases by a factor of 5 when the Fe abundance increases from [Fe/H] = 0.0 dex to [Fe/H] = 0.3 dex. This high probability, together with the fact that HD 80606 already hosts a giant planet and given the very similar stellar parameters with HD 80607, suggests that the giant planet formation process in HD 80607 could be also a very plausible hypothesis. The metals missing in HD 80607 compared to HD 80606 could possibly have been used to form this (hypothetic) giant planet. Tucci Maia et al. (2014) make a similar suggestion to explain the slightly different metallicities between the components of the binary system 16 Cyg. Moreover, there are binary systems in which each component hosts a planet and the metallicity results were slightly different between their stars, such as in the system XO-2 (Damasso et al. 2015). Then, probably because of the mutual interactions in this binary system, HD 80606 b became one of the most eccentric planets to date (see e.g. Wu & Murray 2003), while the HD 80607 system may have had its giant planet ejected. In fact, the possible companion around HD 80607 could be an ejected or maybe an undetected (such as a long period) planet. We stress, however, that this is only a speculative comment and should be taken with caution.

Previous works showed that the global frequency of planets in wide binaries is not statistically different from that of planets in single stars, with no significant dependence of the binary separation (Bonavita & Desidera 2007). Also, the properties of planets in wide binaries are compatible with those of planets orbiting single stars, except for a possible increase of high-eccentricity planets (Desidera & Barbieri 2007). However, the presence of closer stellar companions with separation 100−300 AU could modify the evolution of giant planets around binary components (Desidera & Barbieri 2007).

More recently, Wang et al. (2015) studied 84 KOIs (Kepler Object of Interest) with at least one gas giant planet detected within 1 AU and a control sample of field stars in the solar neighborhood. The authors found a dependence of the stellar multiplicity rate (MR) as a function of the stellar separation a. They derived MRs of ∼0%, ∼34%, and >34% for binary separations of $a < 20$ AU, 20 AU $< a <$ 200 AU, and $a >$ 200 AU, respectively. In other words, no stellar companion has been found within 20 AU for Kepler stars with gas giant planets, while gas giant planet formation is not significantly affected by stellar companions beyond 200 AU. Then, this work shows that the binary separation plays a role in close binaries rather than in wide binaries, such as HD 80606 ($a \sim 1000$ AU). This is in agreement with Zuckerman (2014), who found that the presence of a wide stellar companion ($a \geq 1000$ AU) does not diminish the likelihood of a wide-orbit planetary system.

Wang et al. (2015) also studied the possible physical differences between the components of binaries hosting planets. They suggest that the stellar companions of host stars with a planet period $P > 70$ d tend to be fainter than the shorter-period counterparts. However, they caution that this apparent effect may be due to a lack of sensivity for fainter stellar companions and suggest more follow-up observations to support or disprove it.

Using numerical simulations, Wu & Murray (2003) suggest that the high eccentricity of the planet HD 80606 b is probably due to the influence of the companion HD 80607 through a Kozai mechanism[11] combined with a tidal dissipation. On the other hand, Kaib et al. (2013) showed a possible variable nature of wide binaries due to the Milky Way tidal field, including a reshape of their planetary systems. In this scenario, they obtained an instability fraction (i.e. number of planetary ejections within 10 Gyr of evolution) depending on the binary's mass and separation. Using the binary parameters of HD 80606, they obtained a fraction of ∼50% (see their Fig. 2). Although these simulations do not include the possibility of a planet around HD 80607, they showed that the planetary configuration in this binary system could be strongly affected, and the possible ejection of a planet could not be totally ruled out.

[11] The Kozai mechanism are oscilations in the eccentricity and inclination of a planet due to the presence of a remote stellar companion; see e.g. Kozai (1962).

5. Conclusions

Following the aims of this study, we performed a high-precision differential abundance determination in both components of the remarkable binary system HD 80606−HD 80607, in order to detect a possible signature of terrestrial planet formation. Both stars present very similar stellar parameters, which greatly diminishes the errors in the abundance determination and GCE effects. The star HD 80606 hosts a giant (high-eccentricity) planet while there is no planet detected around HD 80607. First, we derived stellar parameters and differential abundances of both stars using the Sun as the reference star. We compared the possible temperature condensation T_c trends of the stars with the solar-twins trend of Meléndez et al. (2009) and then compared the temperature condensation trend with a sample of solar-analogue stars with [Fe/H] ∼ +0.2 dex from Neves et al. (2009). Our calculation included NLTE corrections for O I and Ba II as well as GCE corrections for all chemical species. From these comparisons, we concluded that the stars HD 80606 and HD 80607 do not seem to be depleted in refractory elements, which differs from the case of the Sun (Meléndez et al. 2009). In other words, the terrestrial planet formation would have been less efficient in the stars of this binary system than in the Sun.

Then, we also compared HD 80607 differentially, using HD 80606 as the reference star. HD 80606 was slightly more metal-rich than HD 80607 by +0.014 ± 0.003 dex. However, we do not find a clear difference between refractory and volatile elements nor a significative trend with T_c between both stars. In comparing the stars to each other, the lack of a trend for refractory elements with T_c implies that the presence of a giant planet does not necessarily imprint a chemical signature on its host star, which is similar to the result of Liu et al. (2014) for the binary system HAT-P-1. This is in agreement with Meléndez et al. (2009), who suggest that the presence of close-in giant planets might prevent the formation of terrestrial planets. Finally, we speculate about a possible (ejected or non-detected) planet around HD 80607. We strongly encourage high-precision abundance studies in binary systems with similar components, which is a crucial tool for helping to detect the possible chemical pattern of the planet formation process.

Acknowledgements. We thank the anonymous referee for constructive comments that greatly improved the paper. The authors wish to recognize and acknowledge the very significant cultural role and reverence that the summit of Mauna Kea has always had within the indigenous Hawaiian community. We are most fortunate to have the opportunity to conduct observations from this mountain. The authors also thank Drs. R. Kurucz and C. Sneden for making their codes available to us.

References

Bakos, G. A., Noyes, R. W., Kovács, G., et al. 2007, ApJ, 656, 552
Bedell, M., Meléndez, J., Bean, J. L., et al. 2014, ApJ, 795, 23
Beirao, P., Santos, N. C., Israelian, G., & Mayor, M. 2005, A&A, 438, 251

Bensby, T., Feltzing, S., & Lundström, I. 2004, A&A, 415, 155
Bergemann, M. 2008, Phys. Scr. T., 133, 014013
Bergemann, M., Pickering, J., & Gehren, T. 2010, MNRAS, 401, 1334
Bonavita, M., & Desidera, S. 2007, A&A, 468, 721
Castelli, F., & Kurucz, R. 2003, New Grids of ATLAS9 Model Atmospheres, held at Uppsala, Sweden, 2002, eds. N. Piskunov, W. W. Weiss, & D. F. Gray, IAU Symp., 210, A20
Cochran, William, D., Hatzes, A. P., Butler, R. P., & Marcy, G. W. 1997, ApJ, 483, 457
Damasso, M., Biazzo, K., Bonomo, A., et al. 2015, A&A, 575, A111
Desidera, S., & Barbieri, M. 2007, A&A, 462, 345
Desidera, S., Gratton, R. G., Scuderi, S., et al. 2004, A&A, 420, 683
Desidera, S., Gratton, R. G., Lucatello, S., & Claudi, R. U. 2006, A&A, 454, 581
Dommanget, J., & Nys, O. 2002, The Catalog of the Components of Double and Multiple Stars (CCDM), Second Edition, Vizier Online Data Catalog I/274
Ecuvillon, A., Israelian, G., Santos, N. C., et al. 2006, A&A, 445, 633
Epstein, C., Johnson, J., Dong, S., et al. 2010, ApJ, 709, 447
Fabbian, D., Asplund, M., Barklem, P., Carlsson, M., & Kiselman, D. 2009, A&A, 500, 1221
Fischer, D., & Valenti, J. 2005, AJ, 622, 1102
Fossey, S., Waldmann, I., & Kipping, D. 2009, MNRAS, 396, L16
Gilli, G., Israelian, G., Ecuvillon, A., Santos, N. C., & Mayor, M. 2006, A&A, 449, 723
Gonzalez, G., & Laws, C. 2007, MNRAS, 378, 1141
González Hernández, J., Delgado Mena, E., Sousa, S. G., et al. 2013, A&A, 552, A6
Gratton, R. G., Bonanno, G., Claudi, R. U., et al. 2001, A&A, 377, 123
Jofré, E., Petrucci, R., Saffe, C., et al. 2015, A&A, 574, A50
Johansson, S., Litzén, U., Lundberg, H., & Zhang, Z. 2003, ApJ, 584, L107
Kaib, N., Raymond, S., & Duncan, M. 2013, Nature, 493, 381
King, R., Parker, R., Patience, J., & Goodwin, S. 2012, MNRAS, 421, 2025
Koleva, M., & Vazdekis, A. 2012, A&A, 538, A143
Korotin, S., Mishenina, T., Gorbaneva, T., & Soubiran, C. 2011, MNRAS, 415, 2093
Kozai, Y. 1962, AJ, 67, 591
Kratter, K. M. 2011, in Evolution of Compact Binaries, eds. L. Schmidtobreick, M. R. Schreiber, & C. Tappert (San Francisco, CA: ASP), ASP Conf. Ser., 447, 47
Kurucz, R. L. 1993, ATLAS9 Stellar Atmosphere Programs and 2 km s^{-1} grid, Kurucz CD-ROM No. 13 (Cambridge, MA: Smithsonian Astrophysical Observatory)
Kurucz, R., & Bell, B. 1995, Atomic Line Data, Kurucz CD-ROM No. 23 (Cambridge, MA: Smithsonian Astrophysical Observatory)
Lambert, D. L. 1978, MNRAS, 182, 249
Laughlin, G., Deming, D., Langton, J., et al. 2009, Nature, 457, L562
Laws, C., & Gonzalez, G. 2001, ApJ, 553, L405
Liu, F., Asplund, M., Ramírez, I., Yong, D., & Meléndez, J. 2014, MNRAS, 442, L51
Lodders, K. 2003, AJ, 591, 1220
Mashonkina, L., Korn, A., & Przybilla. N. 2007, A&A, 461, 261
Meléndez, J., Asplund, M., Gustafsson, B., & Yong, D. 2009, AJ, 704, L66
Meléndez, J., Ramírez, I., Karakas, A., et al. 2014, AJ, 791, 14
Mollá, M., Cavichia, O., & Gibson, B. 2015, MNRAS, 451, 3693
Mortier, A., Santos, N. C., Sousa, S. G., et al. G. 2013, A&A, 558, A106
Moutou, C., Hébrard, G., Bouchy, F., et al. 2009, A&A, 498, L5
Naef, D., Latham, D. W., Mayor, M., et al. 2001, A&A, 375, L27
Neves, V., Santos, N. C., Sousa, S. G., Correia, A. C. M., & Israelian, G. 2009, A&A, 497, 563
Pont, F., Hébrand, G., Irwin, J., et al. 2009, A&A, 502, 695
Ramírez, I., Allende Prieto, C., & Lambert, D. 2007, A&A, 465, 271
Ramírez, I., Asplund, M., Baumann, P., Meléndez, J., & Bensby, T. 2010, A&A, 521, A33
Ramírez, I., Meléndez, J., Cornejo, D., Roederer, I., & Fish, J. 2011, AJ, 740, 76
Raymond, S., Armitage, P., Moro-Martín, A., et al. 2011, A&A, 530, A62
Reiputh, B., & Mikkola, S. 2012, Nature, 492, 221
Reiputh, B., Guimaraes, M., Connelley, M., & Bally, J. 2007, AJ, 134, 2272
Saffe, C. 2011, Rev. Mex. Astron. Astrofis., 47, 3
Saffe, C., & Levato, H. 2014, A&A, 562, A128
Santos, N. C., Israelian, G., & Mayor, M. 2004, A&A, 415, 1153
Santos, N. C., Israelian, G., Mayor, M., et al. 2005, A&A, 437, 1127
Schuler, S., Cunha, K., Smith, V., et al. 2011, ApJ, 737, L32
Sneden, C. 1973, ApJ, 184, 839
Sousa, S. G., Santos, N. C., Mayor, M., et al. 2008, A&A, 487, 373
Steffen, J., Ragozzine, D., Fabycky, D., et al. 2012, Proc. Nat. Acad. Sci. USA, 109, 7982
Takeda, Y. 2003, A&A, 402, 343
Takeda, Y. 2005, PASJ, 57, 83
Tayouchi, D., & Chiba, M. 2014, AJ, 788, 89
Teske, J., Schuler, S., Cunha, K., Smith, V., & Griffith, C. 2013, ApJ, 768, L12
Tucci Maia, M., Meléndez, J., & Ramírez, I. 2014, ApJ, 790, L25
Udry, S., Mayor, M., Benz, W., et al. 2006, A&A, 447, 361
Veras, D., & Armitage, P. 2005, ApJ, 620, L111
Veras, D., & Armitage, P. 2006, ApJ, 645, 1509
Vogt, N., Schmidt, T., Neuhäuser, R., et al. 2012, A&A, 546, A63
Wang, J., Fischer, D., Horch, E., & Xie, J. 2015, ApJ, 806, 248
Wu, Y., & Murray, N. 2003, ApJ, 589, 605
Zuckerman, B. 2014, ApJ, 791, L27

Pages 10 to 17 are available in the electronic edition of the journal at http://www.aanda.org

Table 1. Line list used in this work.

Element	λ [Å]	EP [eV]	log gf [dex]	EW_1 [mÅ]	EW_2 [mÅ]	EW_{Sun} [mÅ]
6.00	5052.167	7.680	−1.240	42.0	39.4	33.6
6.00	6587.610	8.540	−1.050	16.6	14.8	12.1
8.00	7771.944	9.150	0.370	65.7	58.4	66.9
8.00	7774.166	9.150	0.220	61.5	59.3	62.1
8.00	7775.388	9.150	0.000	49.8	47.2	45.0
11.00	4751.822	2.100	−2.080	36.7	38.5	15.7
11.00	5148.838	2.100	−2.040	31.0	31.7	13.8
11.00	6154.225	2.100	−1.550	75.3	80.6	39.2
11.00	6160.747	2.100	−1.250	91.8	94.1	56.9
12.00	4730.040	4.340	−2.390	112.1	108.7	68.6
12.00	5711.088	4.340	−1.730	147.0	144.6	106.6
12.00	6318.717	5.110	−1.950	62.1	63.8	37.3
12.00	6319.236	5.110	−2.160	52.1	51.5	24.2
13.00	5557.070	3.140	−2.210	25.5	25.6	13.4
13.00	6696.018	3.140	−1.480	62.3	64.7	36.0
13.00	6698.667	3.140	−1.780	47.0	48.6	20.8
14.00	5488.983	5.610	−1.690	38.1	36.8	18.5
14.00	5517.540	5.080	−2.500	24.6	23.6	12.2
14.00	5645.611	4.930	−2.040	56.7	56.7	35.8
14.00	5665.554	4.920	−1.940	65.0	65.5	39.3
14.00	5684.484	4.950	−1.550	81.2	80.6	61.0
14.00	5690.425	4.930	−1.770	67.7	67.6	48.5
14.00	5701.104	4.930	−1.950	58.6	56.1	40.3
14.00	5753.640	5.620	−1.330	71.6	72.7	43.5
14.00	5772.145	5.082	−1.653	74.1	74.7	51.8
14.00	5793.073	4.930	−1.960	64.7	62.2	42.9
14.00	5948.540	5.080	−1.208	108.8	108.3	84.4
14.00	6125.021	5.610	−1.500	51.2	49.6	31.7
14.00	6145.015	5.620	−1.410	59.4	58.8	38.7
14.00	6195.460	5.870	−1.666	33.8	34.2	15.2
14.00	6243.823	5.620	−1.270	61.8	59.2	43.9
14.00	6244.476	5.620	−1.320	71.4	70.4	45.4
14.00	6741.630	5.980	−1.650	28.6	27.8	15.2
14.00	7034.903	5.870	−0.780	81.6	82.4	62.8
14.00	7405.770	5.614	−0.720	112.3	111.8	88.7
16.00	4695.443	6.530	−1.830	12.0	12.6	8.2
16.00	6046.000	7.870	−0.150	28.4	24.8	20.3
16.00	6052.656	7.870	−0.400	17.8	16.9	13.2
16.00	6743.540	7.870	−0.600	12.6	10.8	9.7
20.00	5260.387	2.520	−1.720	52.2	54.1	32.5
20.00	5261.710	2.520	−0.680	127.8	131.5	100.6
20.00	5512.980	2.930	−0.460	114.2	116.0	83.8
20.00	5590.114	2.520	−0.570	110.9	113.6	92.8
20.00	5867.562	2.930	−1.570	42.5	43.5	23.5
20.00	6156.020	2.520	−2.497	19.8	19.8	8.7
20.00	6161.297	2.520	−1.270	82.9	84.9	59.5
20.00	6166.439	2.520	−1.140	94.1	95.8	69.6
20.00	6169.550	2.520	−0.580	139.9	141.8	108.7
20.00	6455.598	2.520	−1.340	80.3	82.6	55.2
20.00	6471.662	2.530	−0.690	112.6	115.6	91.0
20.00	6499.650	2.520	−0.820	102.9	105.2	85.5
21.00	4743.821	1.450	0.350	24.9	26.8	9.2
21.00	5081.570	1.450	0.300	25.0	27.3	7.4
21.00	5520.497	1.860	0.550	16.9	17.9	6.1
21.00	5671.821	1.450	0.550	40.2	42.6	14.7
21.10	5657.870	1.510	−0.300	77.6	75.6	65.7
21.10	5669.055	1.500	−1.200	48.6	47.4	36.4
21.10	5684.190	1.510	−0.950	50.9	49.9	37.7
21.10	6245.630	1.510	−1.030	49.2	48.6	35.2
21.10	6279.760	1.500	−1.200	42.8	40.9	30.1
21.10	6320.843	1.500	−1.850	14.3	13.7	7.6
21.10	6604.578	1.360	−1.150	52.5	52.0	35.5

Notes. The columns present the element, wavelength λ, excitation potential (EP), log gf, equivalent widths of HD 80606, HD 80607, and Sun (EW_1, EW_2, and EW_{Sun}). The abundances of lines without EWs are measured using synthetic spectra.

Table 1. continued.

Element	λ [Å]	EP [eV]	log gf [dex]	EW_1 [mÅ]	EW_2 [mÅ]	EW_{Sun} [mÅ]
22.00	4617.280	1.750	0.450	85.6	88.1	64.1
22.00	4645.190	1.730	−0.670	40.8	44.8	21.7
22.00	4656.470	0.000	−1.310	91.4	95.6	68.4
22.00	4758.120	2.250	0.430	61.4	63.2	43.0
22.00	4759.272	2.260	0.510	66.3	67.6	47.0
22.00	4778.258	2.240	−0.220	35.3	35.3	15.4
22.00	4820.410	1.500	−0.440	66.7	69.2	43.0
22.00	4999.500	0.830	0.270	135.8	138.4	104.5
22.00	5022.871	0.830	−0.430	93.7	96.4	70.9
22.00	5024.850	0.820	−0.560	98.5	100.7	70.0
22.00	5039.960	0.020	−1.200	100.7	101.0	76.2
22.00	5071.490	1.460	−0.800	57.0	57.2	27.7
22.00	5147.479	0.000	−2.010	59.9	64.1	34.1
22.00	5219.700	0.020	−2.240	59.7	64.5	29.1
22.00	5471.200	1.440	−1.400	21.9	25.2	7.9
22.00	5490.150	1.460	−0.930	42.7	46.7	21.0
22.00	5689.459	2.300	−0.360	29.0	31.1	11.5
22.00	5739.464	2.250	−0.600	20.2	22.1	6.3
22.00	5766.330	3.290	0.326	22.3	23.1	9.0
22.00	5866.452	1.070	−0.840	76.7	79.6	47.6
22.00	6064.630	1.050	−1.959	25.6	27.1	7.8
22.00	6091.174	2.270	−0.420	35.5	37.9	14.7
22.00	6126.217	1.070	−1.420	46.2	49.5	22.4
22.00	6258.104	1.440	−0.350	79.2	82.3	50.4
22.00	6303.753	1.443	−1.509	24.5	25.7	8.0
22.00	6312.234	1.460	−1.496	20.5	23.6	6.8
22.00	6599.104	0.900	−2.029	27.2	29.6	8.8
22.00	6743.130	0.899	−1.630	43.2	47.1	17.8
22.00	7949.150	1.500	−1.456	29.4	32.2	8.2
22.10	4636.330	1.160	−3.150	30.5	27.3	17.6
22.10	4779.985	2.048	−1.260	72.2	76.3	65.2
22.10	4798.532	1.080	−2.670	53.2	52.4	42.6
22.10	4865.611	1.120	−2.810	55.9	54.2	40.7
22.10	4911.193	3.120	−0.540	64.1	64.1	53.3
22.10	5005.160	1.570	−2.720	31.0	31.5	19.6
22.10	5418.767	1.580	−2.110	60.5	59.1	49.4
23.00	4875.442	0.040	−3.375			
23.00	4875.454	0.040	−2.260			
23.00	4875.461	0.040	−2.964			
23.00	4875.468	0.040	−1.420			
23.00	4875.471	0.040	−2.064			
23.00	4875.477	0.040	−2.742			
23.00	4875.483	0.040	−1.561			
23.00	4875.485	0.040	−2.010			
23.00	4875.491	0.040	−2.617			
23.00	4875.495	0.040	−1.725			
23.00	4875.497	0.040	−2.032			
23.00	4875.502	0.040	−2.566			
23.00	4875.505	0.040	−1.923			
23.00	4875.506	0.040	−2.123			
23.00	4875.509	0.040	−2.596			
23.00	4875.511	0.040	−2.178			
23.00	4875.511	0.040	−2.311			
23.00	4875.515	0.040	−2.566			
23.00	5703.555	1.050	−0.777			
23.00	5703.569	1.050	−0.993			
23.00	5703.569	1.050	−1.403			
23.00	5703.580	1.050	−1.242			
23.00	5703.580	1.050	−1.276			
23.00	5703.581	1.050	−2.268			
23.00	5703.589	1.050	−1.250			
23.00	5703.589	1.050	−1.715			
23.00	5703.590	1.050	−1.840			
23.00	5703.596	1.050	−1.414			
23.00	5703.596	1.050	−1.590			

Table 1. continued.

Element	λ [Å]	EP [eV]	log gf [dex]	EW_1 [mÅ]	EW_2 [mÅ]	EW_{Sun} [mÅ]
23.00	5703.601	1.050	−1.414			
23.00	5727.008	1.080	−0.693			
23.00	5727.016	1.080	−1.701			
23.00	5727.022	1.080	−3.003			
23.00	5727.028	1.080	−0.798			
23.00	5727.035	1.080	−1.490			
23.00	5727.040	1.080	−2.605			
23.00	5727.045	1.080	−0.914			
23.00	5727.051	1.080	−1.417			
23.00	5727.056	1.080	−2.400			
23.00	5727.060	1.080	−1.043			
23.00	5727.065	1.080	−1.411			
23.00	5727.069	1.080	−2.303			
23.00	5727.072	1.080	−1.189			
23.00	5727.075	1.080	−1.458			
23.00	5727.078	1.080	−2.303			
23.00	5727.081	1.080	−1.359			
23.00	5727.084	1.080	−1.563			
23.00	5727.086	1.080	−2.458			
23.00	5727.087	1.080	−1.563			
23.00	5727.089	1.080	−1.759			
23.00	5727.091	1.080	−1.826			
23.00	5727.619	1.050	−1.456			
23.00	5727.619	1.050	−1.867			
23.00	5727.653	1.050	−1.753			
23.00	5727.653	1.050	−2.072			
23.00	5727.654	1.050	−1.867			
23.00	5727.681	1.050	−1.753			
23.00	5727.681	1.050	−1.878			
23.00	5727.681	1.050	−9.850			
23.00	5727.701	1.050	−2.054			
23.00	5727.702	1.050	−1.878			
23.00	6039.726	1.063	−0.650			
23.00	6081.417	1.050	−1.814			
23.00	6081.418	1.050	−1.638			
23.00	6081.428	1.050	−1.638			
23.00	6081.428	1.050	−9.610			
23.00	6081.429	1.050	−1.513			
23.00	6081.443	1.050	−1.513			
23.00	6081.443	1.050	−1.832			
23.00	6081.444	1.050	−1.627			
23.00	6081.461	1.050	−1.627			
23.00	6081.462	1.050	−1.216			
23.00	6090.194	1.080	−0.700			
23.00	6090.201	1.080	−0.841			
23.00	6090.207	1.080	−1.005			
23.00	6090.208	1.080	−1.540			
23.00	6090.213	1.080	−1.203			
23.00	6090.213	1.080	−1.344			
23.00	6090.217	1.080	−1.290			
23.00	6090.217	1.080	−1.458			
23.00	6090.220	1.080	−2.655			
23.00	6090.221	1.080	−1.312			
23.00	6090.221	1.080	−1.846			
23.00	6090.223	1.080	−1.403			
23.00	6090.223	1.080	−2.244			
23.00	6090.225	1.080	−1.591			
23.00	6090.225	1.080	−2.022			
23.00	6090.226	1.080	−1.897			
23.00	6090.227	1.080	−1.846			
23.00	6090.227	1.080	−1.876			
23.00	6111.592	1.042	−1.701			
23.00	6111.632	1.042	−1.224			
23.00	6111.656	1.042	−1.224			
23.00	6111.696	1.042	−1.370			

Table 1. continued.

Element	λ [Å]	EP [eV]	log gf [dex]	EW_1 [mÅ]	EW_2 [mÅ]	EW_{Sun} [mÅ]
23.00	6119.528	1.063	−0.360			
23.00	6199.149	0.286	−2.133			
23.00	6199.167	0.286	−2.238			
23.00	6199.182	0.286	−2.354			
23.00	6199.197	0.286	−2.483			
23.00	6199.201	0.286	−3.141			
23.00	6199.209	0.286	−2.629			
23.00	6199.212	0.286	−2.930			
23.00	6199.221	0.286	−2.799			
23.00	6199.221	0.286	−2.857			
23.00	6199.229	0.286	−2.851			
23.00	6199.230	0.286	−3.003			
23.00	6199.235	0.286	−2.898			
23.00	6199.238	0.286	−3.266			
23.00	6199.240	0.286	−3.003			
23.00	6199.243	0.286	−3.199			
23.00	6199.246	0.286	−4.443			
23.00	6199.251	0.286	−4.045			
23.00	6199.253	0.286	−3.840			
23.00	6199.253	0.286	−3.898			
23.00	6199.255	0.286	−3.743			
23.00	6199.255	0.286	−3.743			
23.00	6242.798	0.262	−2.054			
23.00	6242.798	0.262	−2.521			
23.00	6242.829	0.262	−2.375			
23.00	6242.837	0.262	−2.375			
23.00	6242.852	0.262	−2.396			
23.00	6242.868	0.262	−2.852			
23.00	6243.045	0.300	−2.712			
23.00	6243.060	0.300	−2.497			
23.00	6243.075	0.300	−2.420			
23.00	6243.087	0.300	−1.649			
23.00	6243.087	0.300	−2.409			
23.00	6243.097	0.300	−1.785			
23.00	6243.099	0.300	−2.452			
23.00	6243.106	0.300	−1.933			
23.00	6243.109	0.300	−2.555			
23.00	6243.114	0.300	−2.092			
23.00	6243.118	0.300	−2.776			
23.00	6243.120	0.300	−2.261			
23.00	6243.125	0.300	−2.428			
23.00	6243.129	0.300	−2.566			
23.00	6243.132	0.300	−2.580			
23.00	6243.140	0.300	−2.712			
23.00	6243.142	0.300	−2.776			
23.00	6243.143	0.300	−2.497			
23.00	6243.145	0.300	−2.555			
23.00	6243.146	0.300	−2.420			
23.00	6243.146	0.300	−2.452			
23.00	6243.147	0.300	−2.409			
23.00	6285.160	0.275	−1.540			
24.00	4708.017	3.170	0.090	71.2	72.8	54.6
24.00	4767.860	3.560	−0.600	32.0	33.5	16.3
24.00	4789.340	2.540	−0.350	86.2	86.9	64.8
24.00	4801.047	3.120	−0.130	68.7	70.5	47.9
24.00	4936.335	3.110	−0.250	65.7	68.5	44.2
24.00	5214.140	3.370	−0.740	32.1	33.5	16.1
24.00	5238.964	2.710	−1.270	34.0	36.8	14.9
24.00	5247.566	0.960	−1.590	104.6	107.7	81.4
24.00	5272.007	3.450	−0.420	43.7	44.5	24.0
24.00	5287.200	3.440	−0.870	24.5	26.8	11.0
24.00	5628.621	3.420	−0.760	31.5	32.3	13.8
24.00	5783.080	3.320	−0.430	52.0	55.5	32.2
24.00	5783.870	3.320	−0.290	71.7	75.2	44.1
24.00	5787.930	3.322	−0.080	68.3	70.5	45.7

Table 1. continued.

Element	λ [Å]	EP [eV]	log gf [dex]	EW_1 [mÅ]	EW_2 [mÅ]	EW_{Sun} [mÅ]
24.00	6330.100	0.941	−2.900	53.9	56.4	25.8
24.00	6882.477	3.438	−0.375	59.5	62.6	32.5
24.10	5237.328	4.070	−1.090	60.6	59.7	52.5
25.00	4709.690	2.886	−1.096			
25.00	4709.698	2.886	−2.088			
25.00	4709.698	2.886	−2.088			
25.00	4709.705	2.886	−1.267			
25.00	4709.711	2.886	−1.906			
25.00	4709.711	2.886	−1.906			
25.00	4709.717	2.886	−1.452			
25.00	4709.722	2.886	−1.875			
25.00	4709.723	2.886	−1.875			
25.00	4709.728	2.886	−1.644			
25.00	4709.731	2.886	−1.940			
25.00	4709.731	2.886	−1.940			
25.00	4709.735	2.886	−1.819			
25.00	4709.737	2.886	−2.138			
25.00	4709.737	2.886	−2.138			
25.00	4709.740	2.886	−1.883			
25.00	4739.068	2.939	−1.632			
25.00	4739.069	2.939	−1.155			
25.00	4739.087	2.939	−1.530			
25.00	4739.088	2.939	−1.704			
25.00	4739.089	2.939	−1.632			
25.00	4739.101	2.939	−1.662			
25.00	4739.102	2.939	−3.240			
25.00	4739.103	2.939	−1.530			
25.00	4739.111	2.939	−2.030			
25.00	4739.112	2.939	−1.662			
25.00	5004.892	2.918	−1.630			
26.00	4745.800	3.650	−1.270	97.2	99.1	77.3
26.00	4749.950	4.560	−1.240	55.4	56.6	35.9
26.00	4799.410	3.640	−2.130	52.8	53.5	33.4
26.00	4808.150	3.250	−2.690	43.2	44.3	26.0
26.00	4973.090	3.960	−0.770	103.6	108.2	82.6
26.00	5044.211	2.850	−2.060	93.7	95.6	73.0
26.00	5054.642	3.640	−1.920	61.8	62.2	40.3
26.00	5067.140	4.220	−0.860	93.2	94.7	67.8
26.00	5127.679	0.050	−6.120	39.4	42.0	16.9
26.00	5187.910	4.140	−1.260	80.5	82.2	58.3
26.00	5225.525	0.110	−4.790	95.5	98.0	71.8
26.00	5250.208	0.120	−4.940	85.8	88.1	64.6
26.00	5253.460	3.280	−1.570	101.2	101.8	79.2
26.00	5409.130	4.370	−1.060	77.0	76.8	57.7
26.00	5466.987	3.570	−2.230	54.7	54.9	32.7
26.00	5577.020	5.030	−1.460	20.8	22.1	10.4
26.00	5636.696	3.640	−2.560	35.0	35.7	18.8
26.00	5638.262	4.220	−0.770	101.6	101.1	76.1
26.00	5649.987	5.100	−0.800	54.3	54.6	34.8
26.00	5651.469	4.470	−1.750	34.1	34.0	18.2
26.00	5661.348	4.280	−1.760	41.5	42.7	22.5
26.00	5679.023	4.650	−0.750	76.6	78.9	57.9
26.00	5696.089	4.550	−1.780	26.7	27.1	13.0
26.00	5705.464	4.300	−1.360	56.4	55.8	36.8
26.00	5731.760	4.260	−1.200	76.8	78.4	57.4
26.00	5778.453	2.590	−3.440	43.2	44.5	21.8
26.00	5784.660	3.400	−2.530	46.2	48.6	25.5
26.00	5793.914	4.220	−1.620	51.3	53.4	32.1
26.00	5806.730	4.610	−0.950	76.8	79.1	52.9
26.00	5852.220	4.550	−1.230	62.3	62.8	39.5
26.00	5855.076	4.610	−1.480	39.3	40.3	22.5
26.00	5856.090	4.290	−1.460	51.8	52.5	32.9
26.00	5927.789	4.650	−1.040	60.1	59.9	41.6
26.00	5934.655	3.930	−1.070	99.9	101.2	75.9
26.00	6056.005	4.730	−0.400	92.2	93.9	71.4

Table 1. continued.

Element	λ [Å]	EP [eV]	log gf [dex]	EW_1 [mÅ]	EW_2 [mÅ]	EW_{Sun} [mÅ]
26.00	6079.009	4.650	−1.020	64.7	63.9	44.7
26.00	6082.711	2.220	−3.570	55.0	57.6	33.8
26.00	6093.644	4.610	−1.300	49.1	48.5	29.6
26.00	6127.910	4.140	−1.400	69.5	68.3	49.6
26.00	6151.618	2.180	−3.280	70.3	71.5	49.0
26.00	6157.728	4.080	−1.220	79.9	81.3	60.8
26.00	6165.360	4.140	−1.460	61.7	63.7	43.1
26.00	6213.430	2.220	−2.520	102.8	106.8	81.3
26.00	6219.281	2.200	−2.430	116.5	118.3	88.7
26.00	6226.736	3.880	−2.100	49.4	49.9	28.5
26.00	6252.555	2.400	−1.690	153.3	157.8	118.9
26.00	6270.225	2.860	−2.540	73.7	75.2	51.2
26.00	6271.279	3.330	−2.700	41.3	41.8	22.9
26.00	6335.330	2.200	−2.260	121.7	123.9	95.9
26.00	6392.539	2.280	−4.030	35.2	36.4	15.8
26.00	6481.870	2.280	−2.980	85.7	87.0	63.6
26.00	6518.370	2.830	−2.450	76.7	78.6	56.2
26.00	6593.871	2.430	−2.390	109.4	110.2	82.7
26.00	6597.561	4.800	−0.970	62.3	63.1	43.2
26.00	6625.022	1.010	−5.340	34.7	36.6	14.8
26.00	6699.142	4.593	−2.101	18.4	18.8	8.1
26.00	6703.567	2.760	−3.020	60.7	61.7	36.8
26.00	6705.102	4.610	−0.980	69.2	70.3	46.0
26.00	6713.745	4.800	−1.400	37.7	37.9	20.5
26.00	6725.357	4.100	−2.190	33.2	34.6	16.5
26.00	6726.667	4.610	−1.030	66.0	66.4	46.5
26.00	6733.151	4.640	−1.470	45.9	47.2	26.1
26.00	6750.152	2.420	−2.620	98.2	100.9	73.9
26.00	6806.845	2.730	−3.110	58.1	60.1	34.2
26.00	6810.263	4.610	−0.990	70.3	70.5	49.5
26.00	6828.590	4.640	−0.820	77.2	77.8	54.3
26.00	6837.006	4.590	−1.690	33.3	34.1	17.9
26.00	6842.690	4.640	−1.220	58.3	58.0	36.7
26.00	6843.656	4.550	−0.830	83.8	83.8	60.4
26.00	6858.150	4.610	−0.940	69.9	70.9	50.9
26.00	6999.880	4.100	−1.460	75.1	75.5	54.0
26.00	7132.990	4.080	−1.650	63.0	63.1	41.8
26.00	7401.685	4.186	−1.500	60.0	59.9	40.5
26.00	7418.670	4.140	−1.380	71.2	71.5	47.5
26.10	4620.510	2.830	−3.210	60.0	57.9	52.4
26.10	4993.340	2.810	−3.730	44.3	43.4	38.3
26.10	5414.073	3.220	−3.580	34.3	32.8	26.6
26.10	6084.111	3.200	−3.830	25.9	24.8	20.1
26.10	6416.919	3.890	−2.750	47.2	45.4	38.5
26.10	6432.680	2.890	−3.570	46.7	45.7	39.5
26.10	6456.383	3.900	−2.050	67.4	63.6	61.7
26.10	7711.721	3.903	−2.500	53.1	50.2	44.5
27.00	4792.846	3.250	−0.070			
27.00	4813.467	3.213	0.050			
27.00	5212.691	3.512	−0.110			
27.00	5247.911	1.784	−2.070			
27.00	5647.234	2.278	−1.560			
27.00	6093.143	1.739	−2.440			
27.00	6454.990	3.629	−0.250			
28.00	4831.180	3.610	−0.320	91.9	92.4	73.2
28.00	4866.270	3.540	−0.210	102.4	101.3	77.1
28.00	4913.980	3.740	−0.660	75.2	75.2	55.7
28.00	4946.040	3.800	−1.220	51.2	53.0	28.0
28.00	4952.290	3.610	−1.260	54.5	55.7	32.4
28.00	4953.208	3.740	−0.660	75.6	76.2	56.0
28.00	4976.135	3.610	−1.250	51.3	49.7	29.0
28.00	5010.938	3.640	−0.870	65.0	65.6	48.4
28.00	5082.350	3.660	−0.590	99.3	96.8	67.0
28.00	5084.110	3.680	−0.060	108.3	109.8	88.1
28.00	5094.420	3.830	−1.070	47.7	47.3	28.7

Table 1. continued.

Element	λ [Å]	EP [eV]	log gf [dex]	EW_1 [mÅ]	EW_2 [mÅ]	EW_{Sun} [mÅ]
28.00	5157.980	3.610	−1.510	34.4	35.2	16.9
28.00	5578.729	1.680	−2.570	80.5	83.1	57.4
28.00	5589.358	3.900	−1.140	45.2	45.7	28.1
28.00	5593.746	3.900	−0.780	64.7	66.0	43.8
28.00	5625.320	4.090	−0.730	58.4	56.6	37.1
28.00	5628.350	4.090	−1.320	32.1	30.8	14.3
28.00	5638.750	3.900	−1.700	22.7	22.2	9.6
28.00	5641.880	4.110	−1.020	44.8	44.9	23.2
28.00	5643.078	4.160	−1.250	29.9	30.0	14.6
28.00	5694.990	4.090	−0.630	62.0	62.7	42.7
28.00	5748.360	1.680	−3.240	51.1	52.2	27.5
28.00	5754.670	1.930	−1.850	99.5	101.9	78.7
28.00	5805.217	4.170	−0.640	61.6	63.6	40.4
28.00	5847.010	1.676	−3.410	46.2	48.0	22.6
28.00	6086.282	4.270	−0.510	67.1	68.6	43.4
28.00	6111.080	4.088	−0.810	58.5	58.4	33.3
28.00	6119.760	4.270	−1.316	23.5	24.2	10.6
28.00	6128.984	1.677	−3.360	50.1	49.0	25.0
28.00	6130.135	4.270	−0.960	41.4	40.5	21.9
28.00	6175.370	4.089	−0.550	69.1	69.2	49.0
28.00	6176.811	4.090	−0.260	87.5	87.9	62.9
28.00	6177.242	1.830	−3.510	34.2	33.7	13.5
28.00	6186.717	4.110	−0.960	52.0	52.6	30.6
28.00	6204.604	4.090	−1.140	42.2	43.1	21.7
28.00	6223.971	4.105	−1.466	47.8	48.8	27.0
28.00	6230.100	4.110	−1.132	40.3	42.4	19.3
28.00	6322.169	4.154	−1.210	36.6	36.6	18.5
28.00	6360.810	4.170	−1.150	37.0	35.1	16.6
28.00	6378.233	4.154	−1.386	55.0	55.4	31.0
28.00	6598.611	4.236	−0.910	43.2	43.9	24.8
28.00	6635.130	4.420	−0.720	44.8	44.3	23.3
28.00	6643.630	1.680	−2.000	126.8	126.5	92.1
28.00	6767.772	1.830	−2.170	103.4	106.2	78.4
28.00	6772.315	3.660	−0.990	72.6	73.9	49.2
28.00	6842.043	3.658	−1.500	45.0	40.8	24.2
28.00	7715.591	3.700	−1.010	76.3	77.0	50.0
28.00	7727.624	3.680	−0.400	117.5	118.2	91.0
28.00	7748.890	3.700	−0.380	115.6	116.4	85.0
28.00	7797.586	3.890	−0.340	104.0	107.2	74.0
29.00	5218.197	3.814	0.480			
29.00	7933.096	3.783	−0.877			
29.00	7933.098	3.783	−0.877			
29.00	7933.119	3.783	−0.877			
29.00	7933.119	3.783	−0.877			
29.00	7933.134	3.783	−1.576			
29.00	7933.135	3.783	−1.576			
29.00	7933.155	3.783	−0.877			
29.00	7933.157	3.783	−0.877			
38.00	4607.338	0.000	0.283	68.5	69.2	46.9
39.10	4854.867	0.992	−0.380	55.7	55.1	47.7
39.10	4883.685	1.084	0.070	62.3	62.7	56.8
39.10	4900.110	1.033	−0.090	61.7	60.1	54.1
39.10	5087.420	1.084	−0.170	58.3	57.9	47.0
39.10	5200.413	0.992	−0.570	47.8	47.2	37.9
56.00	5853.686	0.604	−2.066			
56.00	5853.687	0.604	−2.066			
56.00	5853.687	0.604	−2.009			
56.00	5853.688	0.604	−2.009			
56.00	5853.689	0.604	−2.215			
56.00	5853.689	0.604	−2.215			
56.00	5853.690	0.604	−1.010			
56.00	5853.690	0.604	−1.466			
56.00	5853.690	0.604	−1.914			
56.00	5853.690	0.604	−2.620			

Table 1. continued.

Element	λ [Å]	EP [eV]	log gf [dex]	EW_1 [mÅ]	EW_2 [mÅ]	EW_{Sun} [mÅ]
56.00	5853.690	0.604	−1.010			
56.00	5853.690	0.604	−1.466			
56.00	5853.690	0.604	−1.914			
56.00	5853.690	0.604	−2.620			
56.00	5853.690	0.604	−1.010			
56.00	5853.691	0.604	−2.215			
56.00	5853.692	0.604	−2.215			
56.00	5853.693	0.604	−2.009			
56.00	5853.693	0.604	−2.009			
56.00	5853.694	0.604	−2.066			
56.00	5853.694	0.604	−2.066			
56.00	6141.725	0.704	−2.456			
56.00	6141.725	0.704	−2.456			
56.00	6141.727	0.704	−1.311			
56.00	6141.727	0.704	−1.311			
56.00	6141.728	0.704	−2.284			
56.00	6141.728	0.704	−2.284			
56.00	6141.729	0.704	−0.503			
56.00	6141.729	0.704	−1.214			
56.00	6141.729	0.704	−0.503			
56.00	6141.729	0.704	−1.214			
56.00	6141.730	0.704	−0.077			
56.00	6141.730	0.704	−0.077			
56.00	6141.730	0.704	−0.077			
56.00	6141.731	0.704	−0.709			
56.00	6141.731	0.704	−1.327			
56.00	6141.731	0.704	−0.709			
56.00	6141.731	0.704	−1.327			
56.00	6141.732	0.704	−0.959			
56.00	6141.732	0.704	−1.281			
56.00	6141.732	0.704	−0.959			
56.00	6141.733	0.704	−1.281			
56.00	6496.898	0.604	−1.886			
56.00	6496.899	0.604	−1.886			
56.00	6496.901	0.604	−1.186			
56.00	6496.902	0.604	−1.186			
56.00	6496.906	0.604	−0.739			
56.00	6496.906	0.604	−0.739			
56.00	6496.910	0.604	−0.380			
56.00	6496.910	0.604	−0.380			
56.00	6496.910	0.604	−0.380			
56.00	6496.916	0.604	−1.583			
56.00	6496.916	0.604	−1.583			
56.00	6496.917	0.604	−1.186			
56.00	6496.918	0.604	−1.186			
56.00	6496.920	0.604	−1.186			
56.00	6496.922	0.604	−1.186			